Paris
France

B20

Improved Oil Recovery From Tensleep Sandstone - Studies of Brine-Rock Interactions by Micro-CT and AFM

E. Lebedeva (Australian National University), T.J. Senden (Australian National University), M. Knackstedt* (Australian National University) & N. Morrow (University of Wyoming)

SUMMARY

Numerous laboratory studies show that oil recovery by waterflooding can depend on the composition of the injected water. In particular, low salinity water injection has been shown to improve oil recovery in both laboratory core floods and field pilot tests. While the presence of clay, crude oil, and an initial water saturation have all been identified as minimal and necessary conditions for increased recovery from clastic rocks, their relationship as well as other relevant conditions remain uncertain. Several recovery mechanisms have been proposed. In recent work improved recovery of Minnelusa crude oil was observed during injection of low salinity coal-bed methane water into Tensleep sandstone. This eolian sandstone is primarily composed of quartz and is pervasively cemented with dolomite and anhydrite. The sandstone has low clay content and is a potential exception to the presence of clays as a necessary condition. The presence of dolomite crystals was previously shown to be associated with the improved oil recovery mechanism. In this paper we make a range of measurements at the pore and molecular scale on Tensleep sandstone to pin down more precisely the possible improved recovery mechanism. Tensleep sandstone was imaged via micro-CT before and after low salinity brine flooding. Local mobilization of the dolomite crystals and anhydrite within the pore space was observed after changing from high to low salinity injection. The effluent water was analysed for cations and anions during high and low salinity injection; results indicate the dissolution of dolomite occurs during low salinity flooding. These results indicate dolomite may adhere to quartz surfaces at high salinity conditions but releases at lower salinity conditions. We have systematically explored the role of surface forces in the adhesion of silica to carbonate surfaces with the Atomic Force Microscope (AFM). AFM studies of the force interaction between quartz and calcite surfaces are reported for a large number of salt pairs at high and low salinity conditions. Little change in the adhesive forces is measured with salinity and no divalent cation effect was observed; increased adhesion was observed only in the presence of sulfates of monovalent cations. DLVO theory and hydration forces do not explain the force measurements. From these results we postulate that the dolomite surface becomes covered in a molecular layer of sulfate. This layer improves adhesion at high salinity, however under low salinity conditions dissolves and increases the opportunity for the dolomite to detach from the quartz surface.

Introduction

Although waterflooding has been by far the most widely applied improved oil recovery technique for over eighty years, the displacement mechanisms that determine recovery efficiency are not well understood. Evidence has accumulated over the last fifteen years that recovery efficiency depends on brine composition (Jadhunandan and Morrow 1995, Yildiz and Morrow, Tang and Morrow SPE, Tang and Morrow JPSE 1999, Webb et al., Zhang Xie and Morrow et al. 2007). Increased recovery is often observed for salinities below about 5000 ppm. Brines below this concentration are referred to as low salinity brines, LSB, and brines of higher salinity as HSB. Laboratory observations of increased recoveries with low salinity brine injection are supported by field tests (Webb 2004, McGuire et al. 2005). Evidence for improved oil recovery due to specific ions have also been reported (Lager et al, 2006, Zhang and Austad, 2006).

Necessary conditions for increased recovery by LSB flooding were the presence of connate water, the presence of clay, and adsorption of polar components from crude oil (Tang and Morrow, 1999) and also the presence of the crude oil/brine interface (Zhang et al. 2006). Sufficient conditions for increased recovery have not yet been established. Many possibilities have been suggested as to the mechanism of increased recovery. However, many uncertainties remain as to the mechanism by which oil is released from within the rock pore space and then recovered.

An exception to the requirement of clay for increased low salinity recovery was recently reported for Tensleep sandstone from Wyoming (Pu et al.2008). This sandstone is eolian and well sorted but is generally heterogeneous from small to large scale because of the presence and varied distribution of interstitial dolomite and anhydrite. The anhydrite is mainly present as pore filling cement whereas the dolomite is commonly distributed as small crystals including pore filling aggregates. The crystals are about an order of magnitude smaller in diameter than the quartz sand grains. The Minnelusa formation of Wyoming is also eolian with comparable depositional history to the Tensleep. The two formations presently account for one third of Wyoming's current oil production. For the essentially clay-free Tensleep sandstone it has been suggested that the dolomite crystals play a role in the low salinity recovery mechanism. If the rock is treated with hydrochloric acid to remove the dolomite crystals, oil production no longer responded to change from HSB to LSB injection (Pu et al. 2008).

In the present work, the nature of the adhesion between the dolomite crystals and the quartz grains is studied at the pore and molecular scales. The local detachment of dolomite and anhydrite is observed from pore scale micro-CT imaging of Tensleep rock after treatment with low salinity brine. The Atomic Force Microscope (AFM) is used to probe the adhesion of quartz/carbonate surfaces in aqueous electrolytes. Specific ion interactions between carbonate and silica are implicated in the detachment of dolomite/anhydrite under LSB injection in the Tensleep formation. Effluent analysis after LSB and HSB flooding provides further evidence that absence of sulphate anions in LSB might lead to dolomite detachment.

Experimental

Materials

Rocks

A sample of the Tensleep sandstone was taken from the Tensleep Formation at the Teapot Dome oilfield in Northern Wyoming, USA. This sandstone is of eolian origin. Petrophysical studies in previous work (Pu et al. 2008) showed that Tensleep sandstone exhibit partial

filling of primary porosity by dolomite and anhydrite cements and almost complete absence of clays. SEM images of fracture surfaces of the sandstone are shown in Fig. 1. Numerous dolomite crystals of the order of 5-10 microns in diameter are evident. The particles are observed aggregated at grain contacts and attached to quartz surfaces (Fig. 1 (a,b,d)). Chemical analysis via XRD shows that the dolomite contains iron in its structure. The presence of iron lends itself to colour the dolomite present an orangey-pink hue. The presence of trace illite is also noted in the section.

Brines

Two brines were prepared from distilled water and reagent grade chemicals. The compositions of the brines were based on the 38651 ppm Minnelusa reservoir brine and a representative 1316 ppm Coalbed Methane Water with low salt concentration; compositions are detailed in Table 1. In the remainder of this paper these two brines will be referred to as the high salinity and low salinity brines (HSB & LSB) respectively.

Table 1: Composition of Resevoir Brine and CBM Water (Pu et al 2008)

Components	Minnelusa formation water (mg/L) (HSB)	CBM Water (mg/L) (LSB)
NaCl	29,803	915.7
KCl	-	28.7
$CaCl_2$	2,104	191.5
$MgCl_2$	-	180.4
Na_2SO_4	5,903	-
Mg_2SO_4	841	-
TDS	38,651	1,316.3

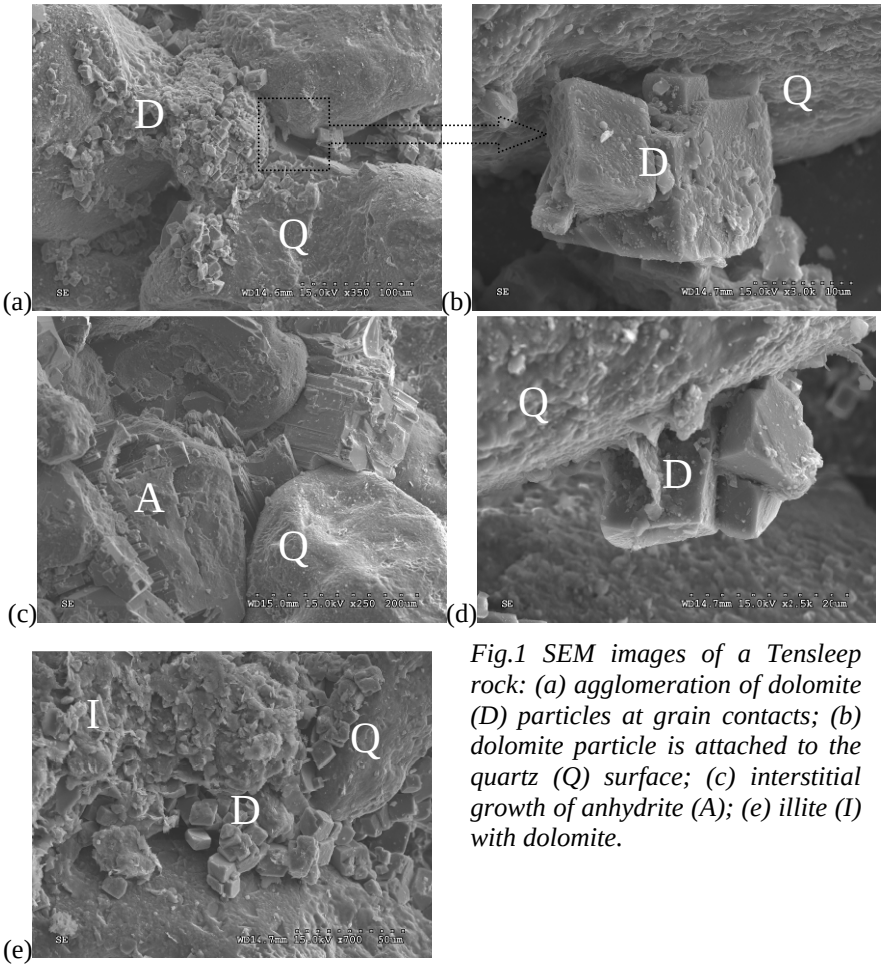

Fig.1 SEM images of a Tensleep rock: (a) agglomeration of dolomite (D) particles at grain contacts; (b) dolomite particle is attached to the quartz (Q) surface; (c) interstitial growth of anhydrite (A); (e) illite (I) with dolomite.

Methods

μ-CT

For the tomographic experiments 4 mm diameter cylinders of Tensleep core ~10 mm in length were extracted from a 4 inch core sample. The tomograms were obtained using the ANU micro-CT facility (Sakellariou et al., 2004); 2880 projections of 2048^2 pixels were acquired; the pixel size was 2.4 microns. Tomograms were typically acquired using filtered Bremsstrahlung with the X-ray source set to a voltage of 80 kV and current of 100μA. The projections were reconstructed and a raw tomographic image obtained. Typically, two data sets were obtained. Firstly, the sample was scanned dry, then vacuum saturated with high salinity brine, flushed with low salinity afterwards and then scanned again.

SEM

High resolution 2D images of the Tensleep sample were made with Hitachi 4300 SE/N Field Emission SEM (2006) at Electron Microscopy Unit at the Australian National University. Backscattered images of fracture surfaces and of thin sections were obtained. XRD analysis was performed on the fracture surfaces.

Atomic Force Microscopy

A Multimode NanoScopeIIIa (Veeco, Inc., Santa Barbara, CA) was used in the current work to image cleaved calcite surface and to measure adhesion forces between silica and calcite with different brines. All experiments were conducted at ambient temperature (20 ± 2^0C). A contact mode silicon cantilever (CSG10: NT-MDT Co., Russia) with a low nominal spring

constant of 0.1 N/m was used in a closed fluid cell. Imaging of the calcite was performed for all solution conditions and there was no discernible variation in calcite topography.

Substrate preparation
Calcite ($CaCO_3$) substrates were prepared by gluing small cleaved pieces onto the steel mounting stub with a pre-set non-volatile epoxy melt (Epon, Shell), followed by cleaning with high-pressure CO_2 snow and then water vapour plasma (18MHz, 10W for 30s, P_{H2O}=0.065 Torr, P_{Ar}=0.02 Torr) immediately prior to use. Silicon cantilevers were cleaned with water vapour plasma to eliminate any organic contamination.

Mass Spectrometer analysis
The ion analysis of the effluent from the Tensleep sandstone after LSB and HSB flooding was performed by Varian Vista AX CCD Simultaneous ICP-AES (cations) and by Dionex Ion Chromotograph Series 4500i (anions).

Results

3D Imaging

Imaging & Phase Separation:
The raw tomographic data set is made up of a 3D array of x-ray attenuation values that are related to the density of the material at each array element. A slice from a tomogram of dry Tensleep is shown in Fig. 2(a) & (b) at different magnifications. The attenuation histogram for the sample is shown in Fig. 3. The range of x-ray densities result in three discernible attenuation peaks. The attenuation peaks are associated with the pore space (low), the quartz grains (intermediate) and the dolomite grains and anhydrite cement (high). Dolomite could not easily be distinguished from anhydrite so the two are combined. Differentiating the attenuation map into these three distinct phases by simple thresholding is problematic. The presence of features with intermediate attenuation (in particular small dolomite particles) and other features at scales below image resolution (e.g. the presence of weathered/partially dissolved grains) results in poorer identification of the three phases by simple thresholding of attenuation (Jones et al., 2007). To analyse the tomograms, a multistage phase identification process is used to label each voxel (Sheppard et al. 2004). The first stage comprises a filter which removes noise while preserving significant features, i.e. the boundary regions between the phases. Regions that are clearly pore space, quartz and dolomite/anhydrite phases are defined on the image data. Phase separation in the more ambiguous intensity regions between these phases is then made using the active contours and watershed methods. The resultant histogram with identification of the three phases is shown in Fig. 3. Image segmentation of the images in Fig. 2(a-b) is shown in Figs. 2 (c-d). The image segmentation seems, to the eye, to capture the phase boundaries accurately.

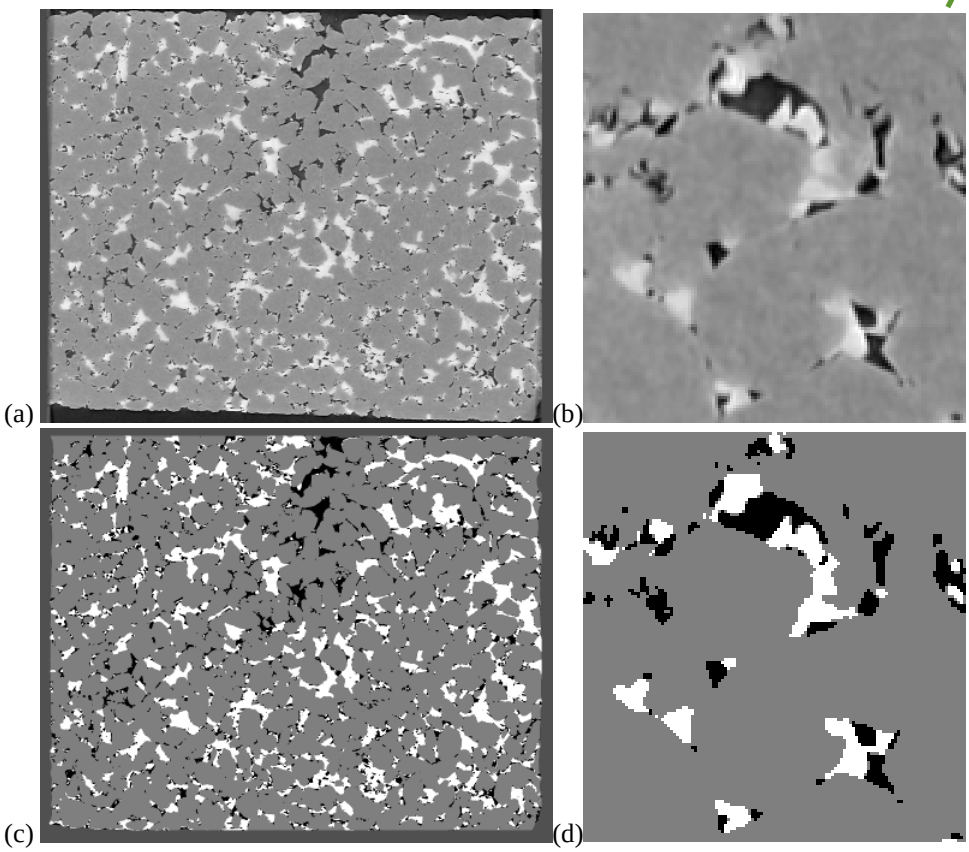

Fig. 2: Gray scale attenuation of a slice through Tensleep sandstone at (a) full image size (4 mm diameter) and (b) zoomed in on a region of 369x408 microns. (c) and (d) show the corresponding three phase segmentation into pore (black), quartz (gray) and dolomite/anhydrite (white) phases of the images.

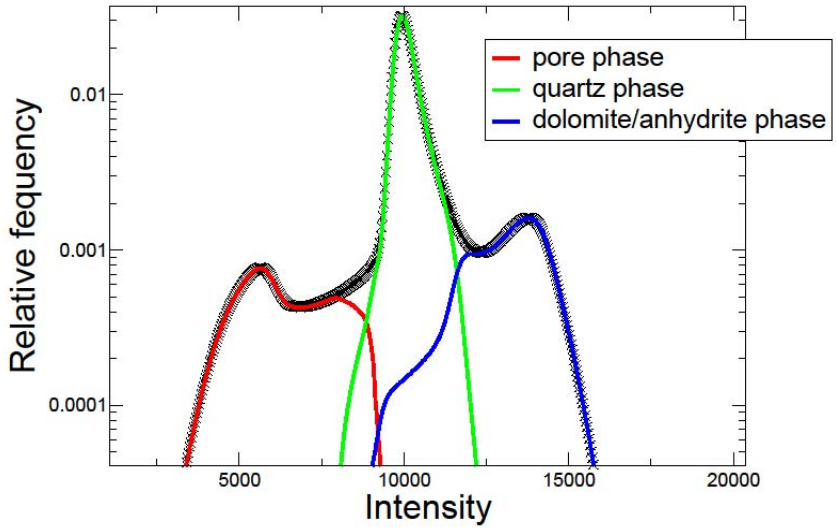

Fig 3. Logarithmic relative frequency vs normalized x-ray attenuation distributions from the Tensleep sample. The black symbols show the overall histogram. The 3 coloured regions illustrate the resultant histogram of the three phases.

A measure of the quality of the image segmentation is based on registering (optimally aligning) higher resolution micrographs, taken by sectioning the actual core scanned, to the original tomogram (Latham et al, 2008). After completion of all micro-CT imaging scans, a thin section is prepared from the imaged sample and the polished surface of the thin section is imaged at high resolution with back scattered electron microscopy (BSEM) and optical microscopy (Fig. 4). This procedure allows preparation of high resolution images and also the direct identification of minerals by optical microscopy. By aligning the high resolution 2D BSEM image with the corresponding slice of the 3D micro-CT data, the quality of the 3D image can be assessed. The results shown in Fig. 4 indicate that the tomographic image provides a reliable representation of the sample and reasonable phase identification.

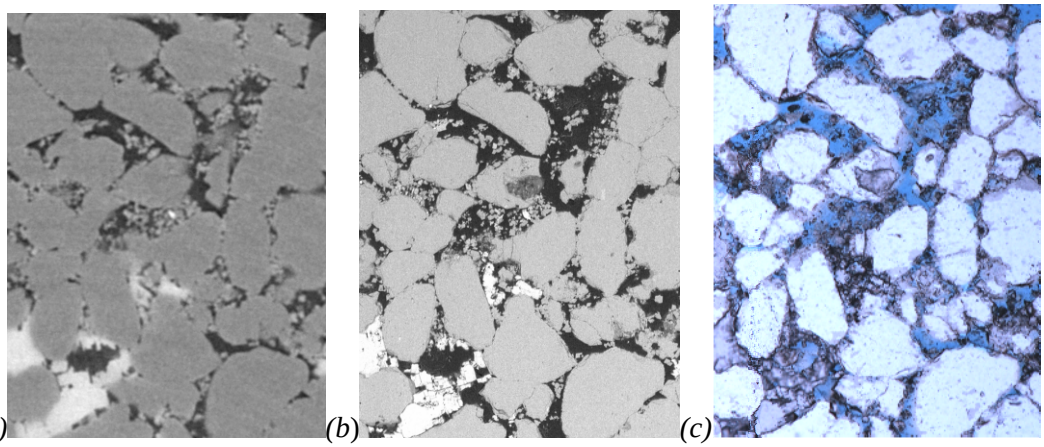

Fig.4. (a) Slice of 3D tomographic image (2.4 microns per voxel) registered to the thin section image from (b) SEM (1.2 microns per pixel) and (c) optical microscopy (1.3 microns per pixel). Sample size is 2mm x 1.5 mm microns. In (a) the pore space and quartz grains, anhydrite cement (bottom left) and dolomite crystals (pore filling particles) are aligned well with the respective phases in (b) and (c).

Imaging after LSB flooding:

The same core was imaged after flooding with LSB. 3D image registration (Latham et al, 2008) allows one to superpose, at voxel resolution, images of the two core images before and after low salinity flooding. This allows direct quantification and comparison of the spatial distribution of the different phases after LSB flooding. There is clear evidence that dolomite/anhydrite phase redistributes after flooding with LSB. Examples of slices through the registered image are shown in Fig. 5. Fig. 6 shows comparisons of 3D visualizations of the image data before and after flooding with LSB. In all cases, movement of the anhydrite cement phase and/or the dolomite particles is evident.

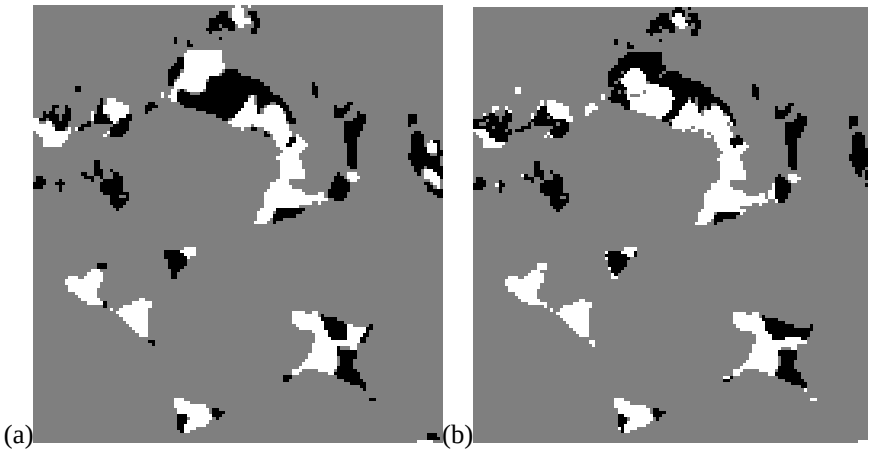

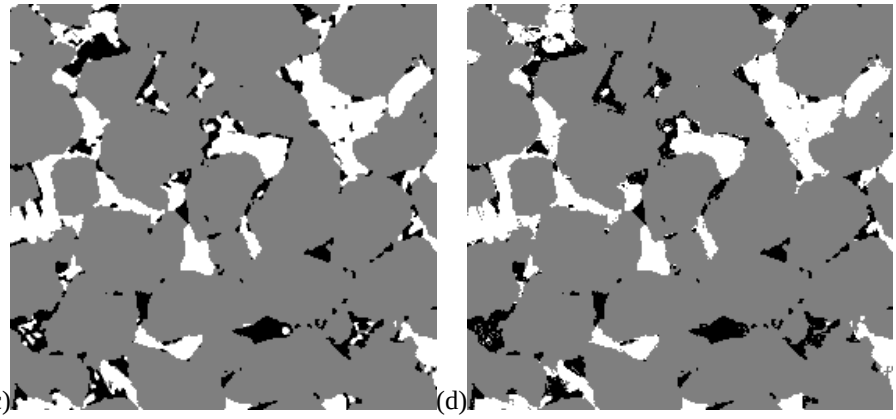

Fig.5: (a),(c) Slices from the original tomogram and (b),(d) corresponding registered slice of same region after flooding with LSB. The size of the images shown are (369x408 microns) for a,b and (819x777 microns) for c,d. The dissolution or redistribution of dolomite particles and/or anhydrite cement is evident from comparison of rock before and after flooding with LSB.

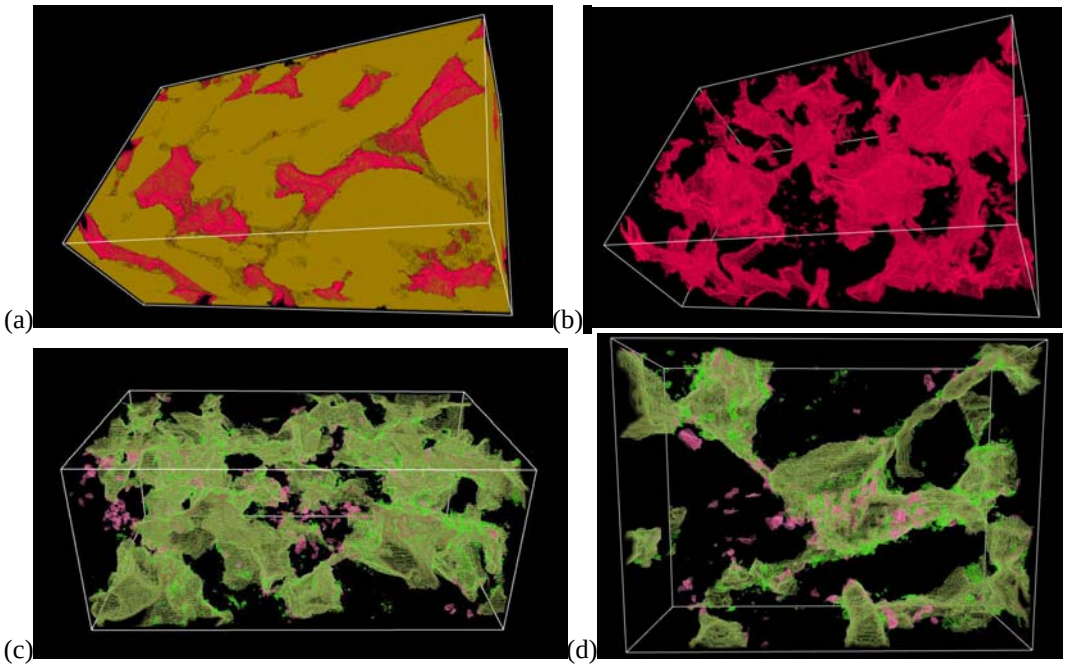

Fig.6. (a) 3D visualisation of a 3D region (816μmx261μmx228μm) in imaged Tensleep sandstone showing quartz (yellow), carbonate (red) with pores (transparent). (b) shows the same volume after removal of the quartz phase; it shows the spatial distribution of carbonate (dolomite/anhydrite) phase , (c) shows volume overlay of the spatial distribution of the carbonate phase in the same volume from the tomogram (816μmx417μmx286μm) before and after LSB flooding. The purple and green phases show respectively the spatial distribution of carbonate before and after LSB flooding. (d) shows a small inset of (c) of volume (483μm x 360μm x 171μm).

AFM measurement of quartz:calcite adhesion

The observation that dolomite adheres to quartz surfaces under HSB conditions, but releases and becomes mobile during LSB flooding leads one to investigate the possible surface forces manifest under these conditions which might explain this observation. The AFM can be used to probe the adhesion of two surfaces in aqueous electrolytes and in this case we employ the silica tip of the cantilever against a carbonate surface and test the adhesion according to a described method (Ducker, 1991). Before we systematically explore the role of these surface

forces it is worth listing which interactions might play a role in the adhesion of silica to carbonate surfaces, and how we aim to test them.

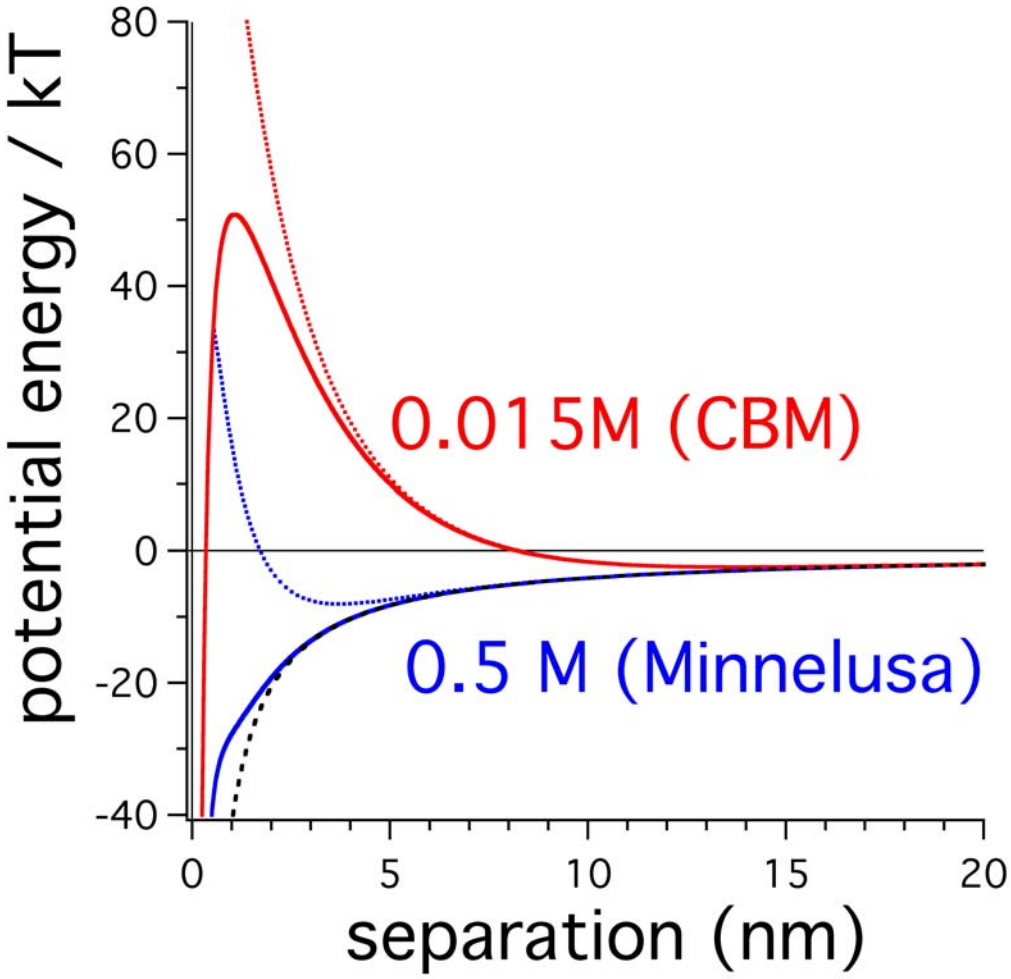

Figure 7. Model interaction potentials for silica and carbonate colloids approaching at 0.5M (similar to salinity of Minnelusa formation brine) and 0.015 M (similar to CBM brine) for their NaCl concentration only, assuming a 200nm radius of silica probe calculated from Poisson-Boltzmann and Lifshitz theories. These curves are indicative of the interactions expected under simple DLVO theory for the mineral surfaces studied here. The additional hydration repulsion, dotted curves, were added as a simple 1nm exponential decay to the DLVO interactions and are indicative only based on literature observations. The black dashed curve shows the van der Waals attraction in isolation.

1) The application of DLVO (Derjaguin-Landau-Verwey-Overbeek) theory (Israelachvili, 1991) suggests that, at HSB conditions, the van der Waals attraction might dominate the total interaction, whereas at LSB the repulsion, due to the overlap of the electrical double layer, dominates (see Fig. 7). DLVO theory assumes that the total interaction is simply the sum of the prevailing surface forces. Van der Waals forces are usually attractive, shown in Fig. 7 as a black dashed line, and are superimposed on the usually repulsive electrostatic double layer, coloured dashed-dotted lines in Fig. 7. The solid coloured lines show the typical interactions for monovalent electrolytes at salinities of the Minnelusa formation brine and the CBM brine. DLVO theory can be extended, again by simply assuming additivity of forces, here with the inclusion of the repulsive short-range hydration force, coloured dotted lines. Note that positive interaction potentials are repulsive (non-adhesive). For potentials less than about +10

kT the interaction generally results in an adhesive contact due to Brownian motion. (kT = Boltzmann's const. times temperature in Kelvin, a measure of thermal energy of a system and hence an indicator of stability). The actual magnitude of the electrostatic repulsion depends very much on the nature and extent of the surface charge. Equally material dependent is the magnitude of the van der Waals attraction. The role of the solution is to control the length-scale (Debye length) of the interaction, which varies as the inverse square-root of concentration. As the valency of the ion increases, the Debye length decreases dramatically. See Israelachvili (1991) for a more complete discussion of DLVO. Thus under DLVO, one would expect an adhesion at HSB and a lack thereof at LSB. It is worth noting here that in general DLVO theory works best at ionic concentrations below 10^{-3} M, whereas at higher concentrations it becomes less reliable. The concentration where improved oil recovery is observed for LSB flooding is loosely considered to be 5000 ppm or 10^{-1} M. In changing the concentration from LSB through to HSB concentrations, as well as changing the valency of the ions we can test the relevance of DLVO to this situation. In this case we have used Na^+, K^+, Ca^{2+}, and La^{3+} to test the effect of valency.

2) At the salinity seen in most reservoirs, the application of DLVO is questionable due to very high concentrations of the brine, and we can look to the non-DLVO forces such as hydration forces. These forces are extremely short range and repulsive in mineral systems (Shubin 1992). In biological systems there are some reports that these forces can be attractive (Leikin et al., 1993) and so they have been investigated here for completeness. To test the importance of this surface force we sought ions with very different ionic radii, but with similar valency or hydrated radii (Nightingale, 1959). For this case, we compare the effect of Li^+, Na^+ and Mg^{2+}. If hydration forces are relevant, these ions should show the greatest hydration effect (Li^+ will show the strongest repulsion).

3) Specific ion effects include all the other surface phenomena one might observe that cannot be explained by 1) or 2) above. They include preferential adsorption of one type of ion over and above ions of similar charge, which can in turn lead to increased or decreased charging. It is possible to imagine that certain ions act to bridge across two surfaces, mediating an adhesive configuration. Like the hydration forces, specific ion effects are also very short range. We tested these effects by studying the chief ionic components of the HSB and LSB used in the Tensleep recovery experiments (Pu et al. 2008); components of the Minnelusa formation brine and CBM brine not already studied above. Principally, one might expect the divalent ions, like Ca^{2+} and Mg^{2+} to bridge the two surfaces. We have also included the sulfate anion as it is present in the Minnelusa brine, but absent from the CBM injection brine.

In varying the concentration and ion type we have been able to explore which of the three proposed mechanisms contribute to the observed changes in adhesion of dolomite to quartz. Figure 8 shows a typical adhesive force curve in which the force required to detach a silica tip from a flat calcite surface is recorded as a function of distance. The adhesive force measured in this way is only semi-quantitative and needs to be referenced to an internal calibration at the time of measurement. In our case we have chosen to normalise each measurement by the average value recorded against pure water. Unlike other colloid probe measurements we therefore do not need to calibrate either the spring constant or the radius of the silica tip. This allows us to rapidly screen the different solutions for adhesion, while foregoing some of the finer detail about the forces upon approach of the two surfaces. In all cases studied, no strong repulsion was noted upon approach and so this data has not been shown here. The absence of repulsion alone means that surface charging is not strongly implicated in the release of dolomite particles and that DLVO is therefore not the reason for the phenomena observed in Tensleep. Indeed, the isoelectric point for calcite is around the pH of the brine solutions

studied (Somasundaran et al., 1967). The lack of observed repulsion is not unreasonable given the low surface charging.

Figure 9 shows the collation of all adhesion results, relative to adhesion measured in water. Immediately the roles of DLVO and hydrations forces can be ruled out. At no stage in the concentration series does calcite develop a substantial surface change, nor is the van der Waals adhesion noticeable. In addition, no short range repulsion typical of hydration forces is seen. Only two ions showed any discernible effects which were consistent with the increased adhesion of dolomite particles under HSB conditions observed in Tensleep. At lower salinities both K^+ and Ca^{2+} show some limited adhesion. As the concentration increases to HSB, K^+ continues to shows a small but significant increase in adhesion and warrants further investigation. Other authors have also noted the specific ion effect of K^+ on calcite. (Bagci et al., 2001). The Ca^{2+} loses its capacity to cause adhesion at HSB due to the re-adsorption of the anion, in this case chloride (Kékicheff et al. 1993). More significant is the effect of SO_4^{2-} which showed a strong increase in adhesion as the concentration crossed the HSB/LSB transition. The presence of sulfate in the HSB and its absence in the CBM water strongly implicates the role of sulphate in the observed detachment of the dolomite/anhydrite from the quartz surfaces. From these results we postulate that the carbonate surface is, to some extent, exchanged for sulfate, a result supported by others (Aikaterini et al. 2008, Cheng et al 1997). They found that, at concentrations of sodium sulphate higher than 10^{-2} M, the anion starts to incorporate into the calcite surface structure by replacing CO_3^{2-}.

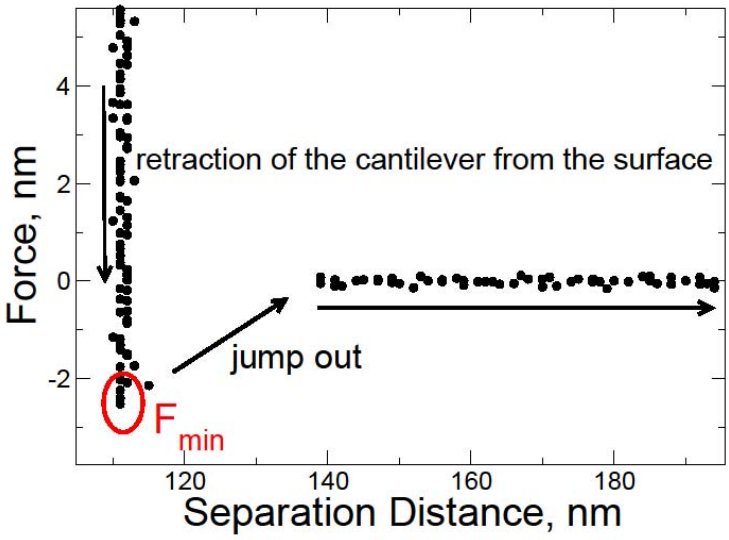

Fig. 8. A typical AFM retraction curve. The curve describes the force acting on the cantilever during retraction. As the cantilever is retracted from the surface an adhesion acts until the surfaces jump apart.

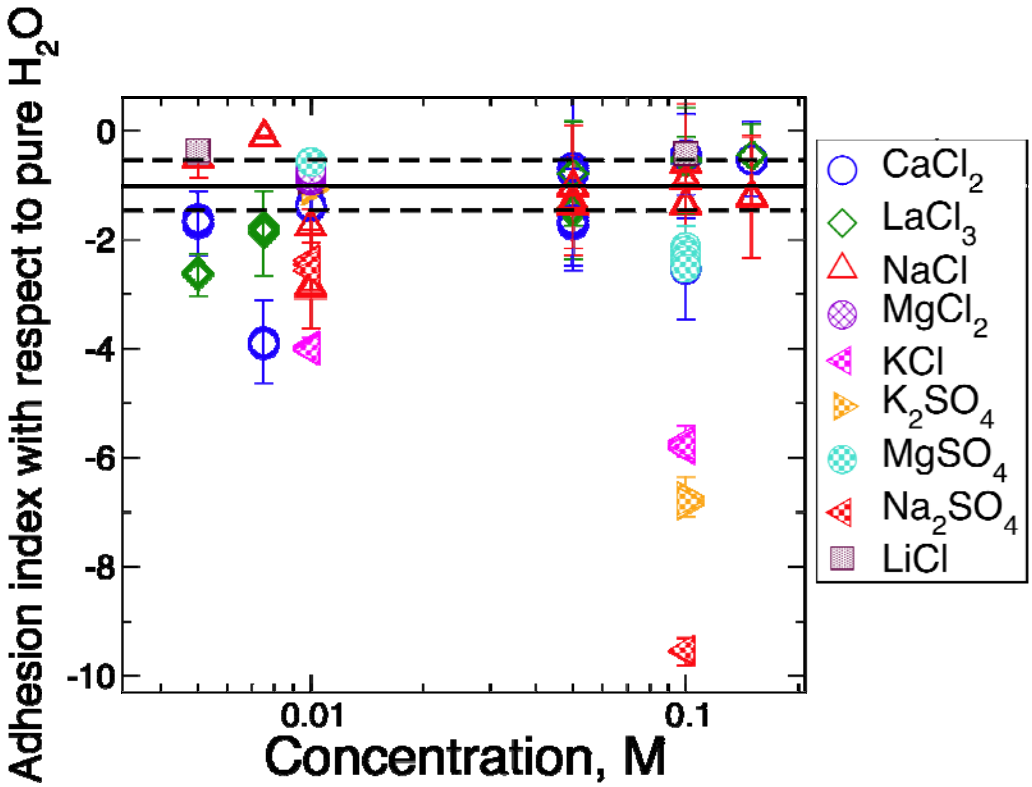

Fig.9 Averaged value of adhesion force between silica and calcite in different brines. All values have been normalised by the average adhesion recorded for pure water.

Mass spectrometer analysis

The concept of dolomite dissolution and role of sulphate is further tested by analysing the effluent after flooding with Minnelusa brine and CBM produced brine. The ion analysis of the LSB flooding with CBM brine indicated a significant presence of sulphate in the effluent despite its absence from the injection brine. This result indicates that anhydrite dissolution is occurring during the LSB flooding. The ion analysis of the LSB effluent also showed the presence of Fe in the effluent; this mineral, again absent from the brine, is found by XRD to be present in the dolomite phase. No Fe was detected after flooding with the Minnelusa formation brine (HSB) or after injection of the LSB with added sulphate. Thus we conclude that iron is released from the dolomite only when the concentration of sulfate falls below a critical value, mostly likely related to the solubility product of anhydrite.

Conclusion & Discussion:

A range of measurements at the pore and molecular scale on Tensleep sandstone have been undertaken to probe more precisely reasons for the observed improved oil recovery under low salinity conditions:

- Micro-CT imaging of Tensleep core before and after low salinity brine flooding was undertaken. Pore scale analysis coupled with image registration led to the observation that the dolomite crystals and anhydrite were locally mobilized within the pore space on changing from high to low salinity injection.

- The ion analysis of the effluent from LSB flooding of Tensleep core with CBM brine indicated a significant presence of sulphate despite its absence from the injection brine. This result indicates that anhydrite dissolution is occurring during the LSB flooding. The ion analysis of the LSB effluent also showed the presence of Fe in the effluent; this mineral, again absent from the brine, is found by XRD to be present in the dolomite phase.
- The AFM is used to probe the adhesion of quartz:calcite surfaces in aqueous electrolytes. The potential interactions which might play a role in the adhesion of silica to carbonate surfaces are tested. DLVO and hydration forces do not explain the adhesion of silica to carbonate surfaces. Specific ion effects do play a role in the interaction. K^+, Ca^{2+} and SO_4^{2-} showed discernible effects which are consistent with the increased adhesion of dolomite particles under HSB conditions observed in Tensleep.

This leads to a proposed model for brine/rock interactions in Tensleep, see Fig. 10. Firstly, and under geological conditions, the dolomite is surface nucleated, the crystallite growing 'keyed-into' the quartz surface. Under HSB conditions this configuration is stable, the balance of ions being sufficient to leave the dolomite at the quartz surface. In the presence of sulfate at HSB conditions the surface of the dolomite becomes exchanged to some extent by SO_4^{2-}. The higher solubility of this coating, in comparison with the parent dolomite, means that in lowering the ionic strength, the crystallite can lose its close conformal connection with the quartz surface. In addition, the native adhesion seen for HSB in the present of sulfate is also diminished. It is worth noting the sulphate recharge can be as little as a molecular film.

In future work we will investigate the dolomite interface directly with the goal of studying the role of specific ion effects on improved oil recovery in Tensleep sandstone. A longer term goal will be to undertake micro-CT imaging studies of oil displacement in Tensleep core after HSB flooding and LSB flooding to observe, at the pore scale, the redistribution of residual oil during improved recovery processes.

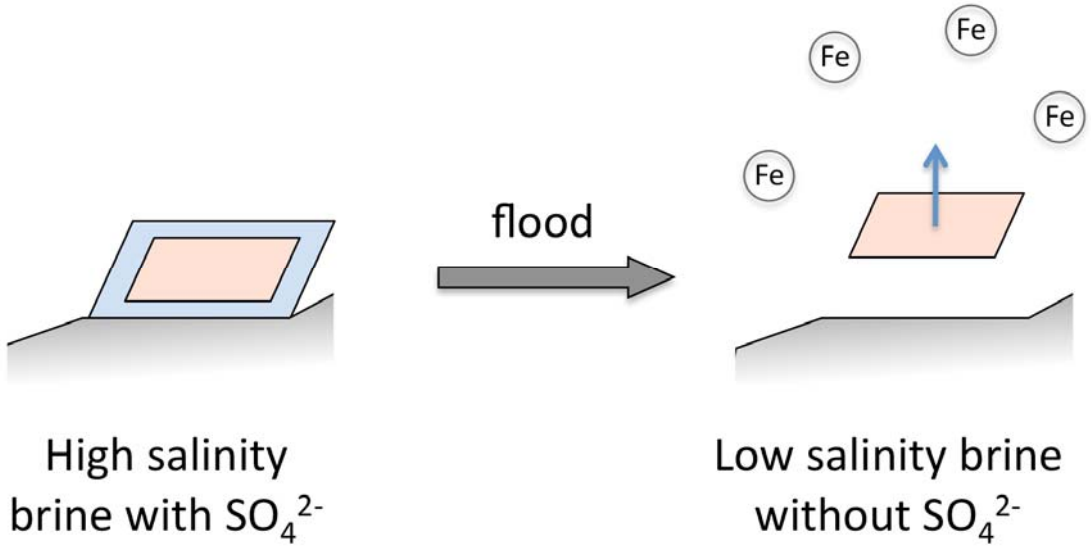

Fig. 10. A schematic showing the suggested mechanism for the detachment of the dolomite particles from the quartz surface in going from HSB (with sulfate enriched layer shown in blue) to LSB (with sulfate absent). The dissolution of the sulfate enriched surface at LSB (via dissolution of anhydrite and similarly by dissolution of a sulphate rich film) allows the particle to more readily detach, simultaneously releasing iron from the dolomite.

Acknowledgement

The authors thank Ajay Limaye and Rob Sok for assistance in image analysis and visualization and the Australian Partnership for Advanced Computing for access to supercomputing infrastructure. This work is supported by the Enhanced Oil Recovery Institute of the University of Wyoming, ARAMCO (Saudi Arabia), BP (UK), Chevron (USA), Shell (Netherlands), StatoilHydro (Norway), and Total (France).

References:

Aikaterini I. Vavouraki, Christine V. Putnis, Andrew Putnis, Petros G. Koutsoukos. [2008] An Atomic Force Microscopy study of the growth of calcite in the presenceof sodium sulphate. *Chemical Geology* 253 243–251.

Bagci, S., Kok, V.M., Turksoy, U. [2001] Effect of brine composition on oil recovery by waterflooding. *Petroleum Science and Technology*, 19:3, 359-372.

Cheng, L., Lyman, P.F., Sturchio, N.C., Bedzyk, M.J., [1997] X-ray standing wave investigation of the surface structure of selenite anions adsorbed on calcite. *Surface Science* 382, 690–695.

Ducker, W.A., Senden, T.J. and R.M. Pashley. [1991] Direct measurement of colloidal forces using an atomic force microscope, *Nature*, 353, 239-241.

Israelachvili J., N. [1991] *Intermolecular and Surface Forces*. 2nd Ed, Academic Press.

Jadhunandan, P.P., Morrow, N.R. [1995] Effect of wettability on waterflood recovery for crude-oil/brine/rock systems. *SPE Reservoir Engineering.* 10, (1) 40-46.

Jones, A.C., C. H. Arns, A. P. Sheppard, D. W. Hutmacher, B. Milthorpe and _M. A. Knackstedt. [2007] *Assessment of Bone ingrowth into Porous Biomaterials using micro-CT, (Biomaterials)*, 28 (15), 2491-2504.

Kékicheff, P., Marcelja, S., Senden, T.J. and Shubin, V.E. [1993], Charge reversal seen in electrical double layer interaction of surfaces immersed in 2:1 Calcium electrolyte, *Journal of Chemical Physics* **99**, 6098-6113 (1993)

Lager,A., Webb, K. J., Black, C. J. J., Singleton,M., Sorbie, K. S. [2006] Low salinity oil recovery - an experimental investigation. The International Symposium of the Society of Core Analysts, Trondheim, Norway.

Leikin, S., Parsegian, V.A., and Rau, D.C. [1993] Hydration forces. *Ann. Rev. Phys. Chem*, 44, 369-95.

Mcguire, P., Chatham J.R., Paskvan, F.K., Sommer, D.M., Carini F.H. [2005] Low salinity oil recovery: an exciting opportunity for Alaska's North Slope. SPE 93903 - *Proceedings of SPE Western regional Meeting*, Irvine, CA.

Nightingale, O.J. [1959] Phenomenological Theory of Ion Salvation. Effective Radii of Hydrated Ions, *J. Phys. Chem*., 69, 1381-87.

Pu, H., Xie, X., Yin, P., Morrow, N.R. [2008] Application of coalbed methan water to oil recovery by low salinity waterflooding. SPE 113410 – *Proceedings of SPE/DOE Improved Oil Recovery Symposium*, Tulsa, Oklahoma.

Sakellariou, A., T.J. Senden, T.J. Sawkins, M.A. Knackstedt, A. Limaye, C.H. Arns, A.P. Sheppard, and R.M. Sok. [2004] An x-ray tomography facility for a wide range of mesoscale physics applications. *U. Bonse (ed.) - Proceedings of SPIE 5535.* Bellingham, WA, 166-171.

Not alphabetical! Latham, S., T. Varslot and A. Sheppard. [2008] Image Registration: Enhancing and calibrating x-ray micro-CT imaging, Society of Core Analysts, *(SCA2008-42): 22nd International Symposium of Core Analysts*, Abu Dhabi.

Sheppard, A.P., R. M. Sok and H. Averdunk. [2004] Techniques for Image enhancement and segmentation of tomographic images.,*Physica A*, 339, 145-151.

Shubin, V. E., Kékicheff, P. [1993] Electrical Double Layer Structure Revisited via a Surface Force Apparatus: Mica Interfaces in Lithium Nitrate Solutions. *Journal of Colloid and Interface Science* 155, 108-123.

Somasundaran, P., Agar, G. E. [1967] The zero point of charge of calcite, *Journal of Colloid and Interface Science*, 24 (4), 433-440.

Tang, G., Morrow, N. R. [1999] Influence of brine composition and fines migration on crude oil/brine/rock interactions and oil recovery. *Journal of Petroleum Science and Engineering*, 24 99-111.

Webb, K.J., Black, C.J.J. and Al-Jeel, H. [2004] Low salinity oil recovery - log inject log. SPE 89379 – *Proceedings of SPE/DOE Fourteenth Symposium on Improved Oil Recovery*, Tulsa, Oklahoma.
Yildiz, H.O., Valat, M., and Morrow, N. R. [1999] Effects of brine composition on wettability and oil recovery of a Prudhoe bay crude oil. *J. Can.Pet. Tech,* 38 (1) 26-31.
Zhang, P. and T. Austad, Wettability and oil recovery from carbonates: effects of temperature and potential determining ions, *Colloids Surf. A, Physicochem. Eng. Asp.* **279** (2006), pp. 179–187.
Zhang, Y., Xie, X. and Morrow, N.R. [2007] Waterflood Performance by Injection of Brine With Different Salinity for Reservoir Cores. SPE_109849 – *Proceedings of SPE Annual Technical Conference and Exhibition*, Anaheim, CA.
Zhang, Y., Morrow, N.R. [2006] Comparison of secondary and tertiary recovery with change in injection brine composition for crude oil/sandstone combinations. SPE 99757 – *Proceedings of SPE/DOE Symposium on Improved Oil Recovery*, Tulsa, Oklahoma.